Oral Presentation

The 7th TSME International Conference on Mechanical Engineering
13-16 December 2016

TSME ICOME 2016
Mechanical Engineering Innovation for Green Society

TSF0015

On Airfoil Shape at Reynolds Number of about 100 – 1000

Kazuki ONISHI[1,*], Erika TAKAHASHI[1], Shogo KONDO[1], Hirochika TANIGAWA[2] and Katsuya HIRATA[1]

[1] Depertment of Mechanical Engineering, Doshisha Univ., Kyoto 610-0321, Japan
[2] Depertment of Mechanical Engineering, NIT Maizuru College, Maizuru 625-5511, Japan
[*] Corresponding Author: dup0554@mail4.doshisha.ac.jp, +81-(0)774-65-6455, +81-(0)774-65-6830

Abstract

The aerodynamic characteristics of airfoils have been researched in high Reynolds-number ranges more than 10^6, in a historic context closely related with the developments of airplanes and fluid machineries in the last century. However, our knowledge is not enough at low and middle Reynolds-number ranges. So, in the present study, we have investigated three kinds of airfoils, namely, such two basic airfoils as a flat plate and a NACA0015 together with an iNACA0015 (the NACA0015 placed back to front) which was proposed as a high-performance airfoil for low Reynolds number, in a low-Reynolds-number range of $Re = 1.0\times10^2 – 8.0\times10^2$, using three-dimensional computations and experiments. As a result, we have revealed the effects of attack angle α upon various aerodynamic characteristics such as the lift coefficient C_L, drag coefficient C_D and the lift-to-drag ratio C_L/C_D. Besides, we have visualized the flow structure in three dimensions.

Keywords: Low Reynolds number, Airfoil, Wing, Aerodynamics, Drone

1. Introduction

The airfoil is one of the most elemental devices for flying/swimming robots to control flow and its reacting force, which determines their basic performances. However, the aerodynamic characteristics of the airfoil have been researched mainly in high Reynolds-number ranges more than 10^6, in a historic context closely related with the developments of airplanes and fluid machineries in the last century [1] – [4]. On the other hand, we have been requiring more precise knowledge about the aerodynamic characteristics of the airfoil especially in low Reynolds-number ranges less than 10^6, because of the recent miniaturization of robots such as unmanned aerial vehicles known as UAVs or micro air vehicles known as MAVs [5] & [6], in addition to the importance of insect/bird flight dynamics, small-scale machines like micro fluid machineries and micro combustion engines and so on.

Concerning the aerodynamic characteristics at low Reynolds numbers, there have been several studies [7] – [25]. However, in such low Reynolds number ranges, our knowledge has not been enough yet, due to the laminar-to-turbulent transition with strong nonlinearity which brings us some technical difficulties in the accuracies of analyses, computations and experiments.

Recently, we have investigated such basic two-dimensional airfoils as a flat plate (hereinafter, referred to as FP), a NACA0015 and some flat plates with modified fore-face and back-face geometries at Reynolds numbers Re's $< 1.0\times10^5$, using two- and three-dimensional computations together with wind-tunnel and water-tank experiments [22]. As a result, we have revealed the effect of the Reynolds number Re upon the minimum drag coefficient $C_{D\min}$ at $Re = 1.0\times10^2 – 1.0\times10^5$ about two kinds of basic airfoils. Besides, at $Re = 1.0\times10^2$, we have shown the effects of attack angle α upon various aerodynamic characteristics, discussing those effects on the basis of both near-flow-field information and surface-pressure profiles. Such results suggest the importance of sharp leading edges, which implies the possibility of an inversed NACA0015 (hereinafter, referred to as iNACA0015). Furthermore, concerning the FP, we have revealed the influences of fore-face and back-face geometries upon such effects.

Later, we suppose three kinds of a two-dimensional airfoils with high performance at very low Re's; namely, the iNACA0015 and have examined them at $Re = 1.0\times10^2$ in comparison with such basic airfoils as the FP and the NACA0015 by three-dimensional computations [25].

In the present study, we investigate three kinds of airfoils, namely, such two basic airfoils as a flat plate and a NACA0015 together with an iNACA0015 (the NACA0015 placed back to front) which was proposed as a high-performance airfoil for low Reynolds number, using three-dimensional computations and experiments. Specifically speaking, we focus our attention upon the flow at $Re = 1.0\times10^2 – 8.0\times10^2$. Then, we investigate the effects of attack angle α upon various aerodynamic characteristics such as the lift coefficient C_L, drag coefficient C_D and the lift-to-drag ratio C_L/C_D. In order to discuss the revealed α effects, we visualize the flow around the airfoils using the Q value, the helicity, streamlines and pressure/vorticity distributions around the airfoils at $\alpha = 0 – 24$ deg.

TSF0015

Nomenclature

$2A_F$	flap amplitude (up-to-down) [m]
c	chord length, = characteristic length scale [m]
C_D	drag coefficient
C_L	lift coefficient
C_L/C_D	lift-to-drag ratio
C_p	pressure coefficient
f_F	frap frequency [Hz]
H	physical computational -domain size [m]
H_R	relative helicity, $\equiv (\boldsymbol{v} \cdot \boldsymbol{\omega})/(\|\boldsymbol{v}\| \, \|\boldsymbol{\omega}\|)$
Ma	Mach number
Q	second invariant of velocity gradient tensor [1/s^2]
Re	Reynolds number, $\equiv \rho U_\infty c/\mu$
$Re\,(V_{WT})$	Reynolds number based on V_{WT}, $\equiv \rho V_{WT} c/\mu$
s	wing span [m]
t	flat-plate thickness [m]
t/c	cross-section ratio
$\boldsymbol{v} = (u, v, w)$	flow velocity [m/s]
U_∞	mean flow velocity of uniform mainstream [m/s]
V_{WT}	wing-tip velocity (the maximum over one flap), $\equiv 2\pi A_F f_F$ [m/s]
(x, y, z), (ξ, η, z)	coordinates [m]
α	attack angle [deg.]
α'	corrected α [deg.]
$\Delta\xi_{min}$, $\Delta\eta_{min}$	minimum grid size [m]
ρ	density of fluid [kg/m^3]
μ	viscosity of fluid [Pa s]
$\boldsymbol{\omega} = (\omega_x, \omega_y, \omega_z)$	vorticity [1/s]

2. Method

2.1 Model

Figure 1 shows the present models. They are two kinds of fundamental airfoils such as a FP and a NACA0015, together with a two-dimensional airfoil with high performance at low *Re*; namely, an iNACA0015 (the NACA0015 placed back to front).

All the present three airfoils have a chord length of *c*. The iNACA0015 resembles the optimum shapes for drag minimisation [18] & [19] and for lift maximisation [19], respectively. The iNACA0015 is rather the shape with a sharp edge in front and with a round surface in back.

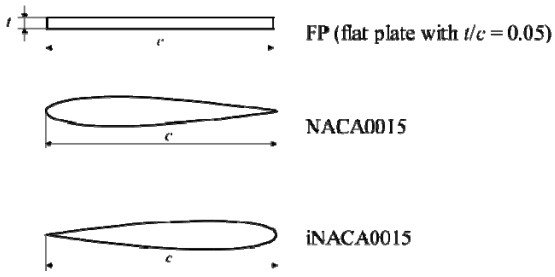

Fig. 1 Models: two-dimensional airfoils.

The FP and the NACA0015 are two-dimensional airfoils with basic and symmetric cross sections: the NACA0015 is a typical streamlined airfoil for high *Re*, and the FP is the simplest thin airfoil with sharp leading and trailing edges. The FP has a cross-section ratio $t/c = 0.05$.

Concerning the iNACA0015, we have shown the importance of sharp leading edges for the improvement of aerodynamic characteristics at very low *Re*, which bring the sharp and very-low pressure drop near the upper fore-face [22]. The former brings the lower-surface higher pressure, and the latter brings the slightly-lower pressure widely-distributed over the middle portion of the upper surface at small α. This importance of sharp leading edges might imply the iNACA0015.

In order to non-dimensionalize all the concerning physical quantities, we consider c as a characteristic length scale and the mean flow velocity U_∞ of uniform mainstream as a characteristic velocity scale. The tested value of *Re* is fixed to 1.0×10^2 in all the present computations.

Now, we survey the flight/swim of actual creatures in low *Re* ranges [25]. Figure 2 summarizes the relation between *Re* or $Re(V_{WT})$ and the chord length c for various flying objects in air, namely, some animals flying in air in addition to the MAVs and so on. The Reynolds number $Re(V_{WT})$ based on wing-tip velocity V_{WT}. We can see that there exit the flights/swims using flapping motion of actual creatures at $Re \simeq 10^2 - 10^3$. This implies the importance to understand the aerodynamics of airfoils even at such a very low *Re* as 10^2, although the lift force is relatively weakened in comparison with the drag force by strong viscous friction.

2.2 Computational procedure

We investigate the above three kinds of airfoils, numerically. The present procedure of computation is as well as [22]. In many actual situations, most of the flow at $Re < 10^6$ could be usually regarded as incompressible and viscous. So, we suppose the incompressible full Navier-Stokes equations in three dimensions. We approximately solve the equations by a finite-difference method using the MAC scheme for velocity/pressure coupling, a third-order-upwind difference scheme in spatial discretization of convective terms, a second-order-central difference scheme in spatial discretization of the other terms and the Euler explicit scheme in a time marching.

The boundary condition on the airfoil surface is viscid. On the outer boundaries of the computational domain, we suppose the Dirichlet condition as $u = U_\infty$, $v = 0$ and $w = 0$. As a spatial grid, we use an O-type staggered grid, which is a boundary-fitted one with a generalized coordinate system (ξ, η). The grid numbers

in the ξ and η directions are 200 and 90, respectively. The minimum grid size $\Delta\eta_{min}$ is $1.0\times10^{-3}c$.

And, a physical computational-domain size H is $28.0c$, where H denotes the diameter of a circular computational domain with its origin O at an airfoil's front.

At a time step $\Delta t = 1.0\times10^{-4}c/U_\infty$, we proceed with the above time-marching computations, during which we monitor both the values of C_D and C_L, to judge whether the total computation time is enough or not for fully-saturated conditions.

Such parameter values as H, $\Delta\xi_{min}$, $\Delta\eta_{min}$ and Δt are determined by many preliminary trials, to achieve negligible influences upon results. We can see that both the influences are negligible at $\Delta\xi_{min}/c \lesssim 0.01$.

2.3 Experimental apparatus

In order to confirm computational results, we conduct experiments for flow visualization. Figure 3 shows photograph of an experimental set-up with a towing water tank and stationary apparatus for $Re = 10^1 - 10^2$. Figure 4 shows photograph of an experimental set-up with a stationary water tank and towing apparatus for $Re = 10^2 - 10^3$. To conclude the present computations are in good agreement with the experiments from a qualitative point of view.

3. Results and Discussion

3.1 Aerodynamic characteristics

Figures 5, 6 and 7 summarize the aerodynamic characteristics of the three airfoils at $Re = 1.0\times10^2$, 4.0×10^2 and $Re = 8.0\times10^2$, respectively. Each figure shows the α effects: namely, C_D, C_L and C_L/C_D are plotted against α in figures (a), (b) and (c), respectively.

At first, we see Fig. 5(a). For all the three airfoils, C_D monotonically and gradually increases with increasing α in the tested range of $\alpha = 0 - 24$ deg. Not only qualitatively but also quantitatively, C_D resembles with one another. Then, C_D can be approximated to a constant value of 0.4 in such a range as $\alpha \lesssim 10$ deg., for all the three airfoils at $Re = 1.0\times10^2$.

Second, we see Fig. 5(b). C_L monotonically increasing α in the tested range of $\alpha = 0 - 24$ deg., for the two airfoils except for the iNACA0015 for which C_L attains the maximum at $\alpha = 22$ deg. On the other hand, the increasing rate $dC_L/d\alpha$ monotonically reduces with increasing α with the constant-$dC_L/d\alpha$ range at small α, for all the three airfoils. From a quantitative point of view, we see obvious discrepancies among the three airfoils, which depend upon α.

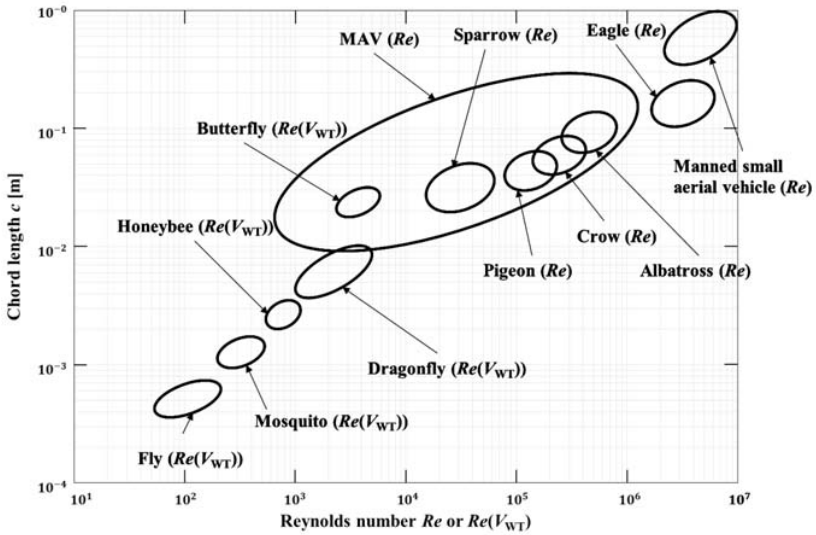

Fig. 2 Relation between Reynolds number Re or $Re(V_{WT})$ and chord length c for various flying objects in air (Hirata et al., 2016).

Third, we see Fig. 5(c). For all the three airfoils, C_L/C_D monotonically increases with increasing α at $\alpha \lesssim 10$ deg. At $\alpha \gtrsim 10$ deg., $d(C_L/C_D)/d\alpha$ monotonically reduces with increasing α. And at a certain α in the range of $\alpha = 16 - 22$ deg., $d(C_L/C_D)/d\alpha$ crosses zero toward negative: namely, C_L/C_D attains the maximum at the certain α. Then, a mild stall appears for each airfoil. From a quantitative point of view, we again see obvious discrepancies among the three airfoils, which depend upon α.

At first, we see Fig. 6(a). For all the three airfoils, C_D monotonically and gradually increases with increasing α in the tested range of $\alpha = 0 - 24$ deg. as well as Fig. 5(a) at $\alpha \lesssim 10$ deg. Not only qualitatively but also quantitatively, C_D resembles with one another. Then, C_D can be approximated to a constant value of 0.2 in such a range as $\alpha < 10$ deg., for all the three airfoils at $Re = 4.0\times10^2$.

Second, we see Fig. 6(b). C_L monotonically increasing α in the tested range of $\alpha = 0 - 24$ deg. And the increasing rate $dC_L/d\alpha$ is constant. From a quantitative point of view, we see obvious discrepancies among the three airfoils at $\alpha > 10$ deg.

Third, we see Fig. 6(c). For all the three airfoils, C_L/C_D monotonically increases with increasing α at $\alpha \lesssim 10$ deg. At $\alpha \gtrsim 10$ deg., $d(C_L/C_D)/d\alpha$ monotonically reduces with increasing α. And at $\alpha = 10$ deg., $d(C_L/C_D)/d\alpha$ crosses zero toward negative: namely, C_L/C_D attains the maximum at $\alpha = 10$ deg.

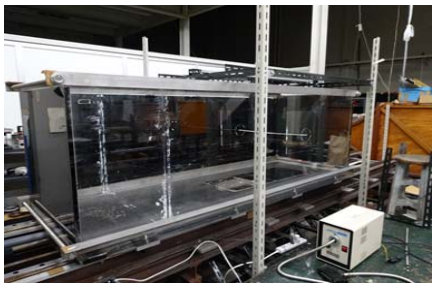

Fig. 3 Photograph of an experimental set-up with a towing water tank and stationary apparatus for $Re = 10^1 - 10^2$.

Fig. 4 Photograph of an experimental set-up with a stationary water tank and towing apparatus for $Re = 10^2 - 10^3$.

Then, a mild stall appears for each airfoil. From a quantitative point of view, we again see obvious discrepancies among the three airfoils, which depend upon α.

At first, we see Fig. 7(a). For all the three airfoils, C_D monotonically and gradually increases with increasing α in the tested range of $\alpha = 0 - 24$ deg. as well as 5(a) and 6(a). Not only qualitatively but also quantitatively, C_D resembles with one another. Then, C_D can be approximated to a constant value of 0.2 in such a range as $\alpha \lesssim 10$ deg., for all the three airfoils at $Re = 8.0\times10^2$.

Second, we see Fig. 7(b). C_L monotonically increasing α in the tested range of $\alpha = 0 - 24$ deg. And the increasing rate $dC_L/d\alpha$ is constant at $\alpha < 10$ deg. From a quantitative point of view, we see obvious discrepancies among the three airfoils, at $\alpha > 10$ deg.

Third, we see Fig. 7(c). For the FP, C_L/C_D monotonically increases with increasing α at $\alpha \lesssim 8$ deg. At $\alpha \gtrsim 8$ deg., $d(C_L/C_D)/d\alpha$ monotonically reduces with increasing α. And at $\alpha = 8$ deg., $d(C_L/C_D)/d\alpha$ crosses zero toward negative: namely, C_L/C_D attains the maximum at $\alpha = 8$ deg. For the NACA0015, C_L/C_D monotonically increases with increasing α at $\alpha \lesssim 15$ deg. For the iNACA0015, C_L/C_D monotonically increases with increasing α at $\alpha \lesssim 10$ deg. At $\alpha \gtrsim 10$ deg., $d(C_L/C_D)/d\alpha$ monotonically reduces with increasing α. And at $\alpha = 10$ deg., $d(C_L/C_D)/d\alpha$ crosses zero toward negative: namely, C_L/C_D attains the maximum at $\alpha = 10$ deg. Then, a mild stall appears for each airfoil.

In summary, at $Re = 1.0\times10^2$, all the aerodynamic characteristics of the three airfoils qualitatively resemble with one another. On the other hand, at $Re = 8.0\times10^2$, C_L/C_D of the three airfoils differs with one another, and the iNACA0015 shows the best performance. Specifically speaking, both the FP and the iNACA0015 attain the highest value of about 3. And, the high C_L/C_D of the NACA0015 appears at larger α than the FP. This suggests better controllability.

Finally, we see the other researchers in Figure 5 and 6 and our previous researchers in Figure 7, comparing to the present computations. In summary, we can confirm the accuracy of the present computations which agree well with such data.

3.2 Flow visualization by analysis

Figures 8, 9 and 10 show samples of 3D computations. More specifically, Figs. 8 and 9 and 10 denote the flows for the FP, the NACA0015 and the iNACA0015, respectively at $\alpha = 24$ deg. Both Figs. 8, 9 and 10 are visualized using iso-Q surfaces with a normalized Q value ($\equiv Qc^2/U_\infty^2$) of 3. The color on the iso-Q surfaces represents relative helicity H_R shown as a legend on the upper right hand of each figure. We

can see all the flows are fully two-dimensional, because of the tubular shapes of the iso-Q surfaces and because of the value of H_R which is zero everywhere. Besides, we should note that all the flows are unsteady.

In summary, the flow around the three airfoils at $Re = 1.0\times10^2$ and 4.0×10^2 and $\alpha = 24$ deg. is unsteady and two-dimensional even at $\alpha = 24$ deg.

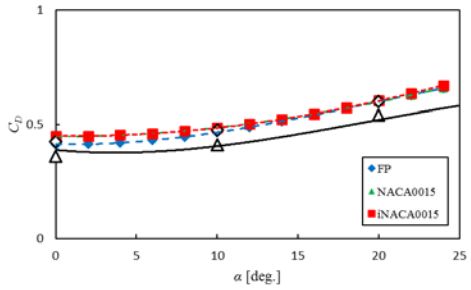

(a) Drag coefficient C_D

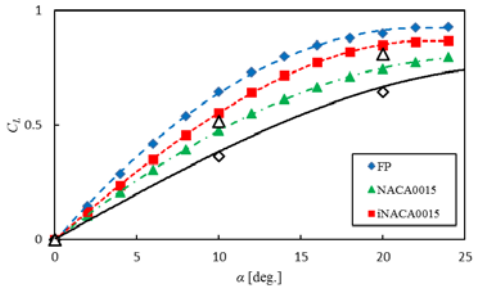

(b) Lift coefficient C_L

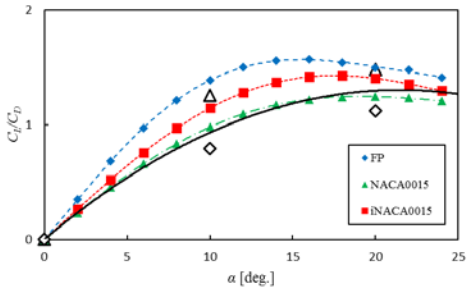

(c) Lift-to-drag ratio C_L/C_D

Fig. 5 Aerodynamic characteristics versus attack angle α at $Re = 1.0\times10^2$. ◆, ▲ and ■ ; 3D computations. - - -, - · - and ····· ; 2D computations by Hirata et al. 2010. ◇; 3D Computations by Taira et al. (2009) (for FP with $AR = 2$ and $t/c = 0.037$ at $Re = 1.0\times10^2$ using a grid size of 200×88×128). ——; Experiments using oil tow tank by Taira et al. (2009) (for FP with $AR = 2$ and $t/c = 0.037$ at $Re = 1.0\times10^2$). △; 2D computations by Sun & Boyd (2004) (for FP with $t/c = 0.05$ at $Re = 135.7$ and $Ma = 0.2$).

On the other hand, the flow around the three airfoils at $Re = 8.0\times10^2$ is unsteady and three-dimensional at $\alpha = 24$ deg.

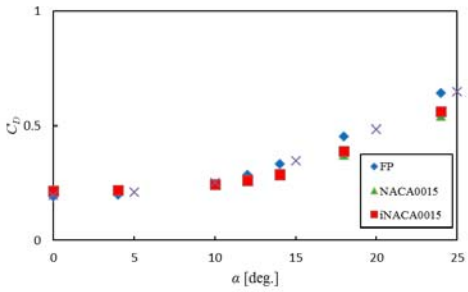

(a) Drag coefficient C_D

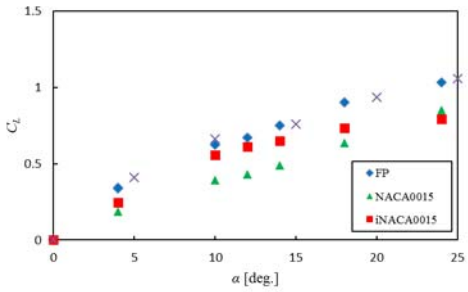

(b) Lift coefficient C_L

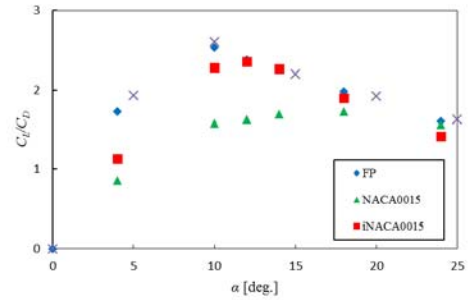

(c) Lift-to-drag ratio C_L/C_D

Fig. 6 Aerodynamic characteristics versus attack angle α at $Re = 4.0\times10^2$. ×; 2D computations by Taira et al. (2009) (for FP with $t/c = 0.037$ at $Re = 3.0\times10^2$).

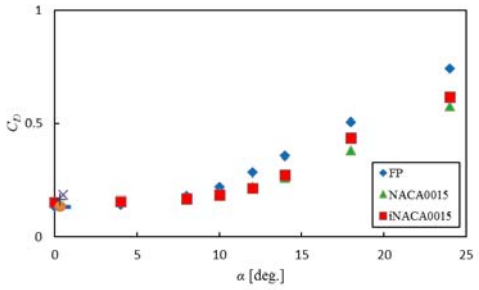

(a) Drag coefficient C_D

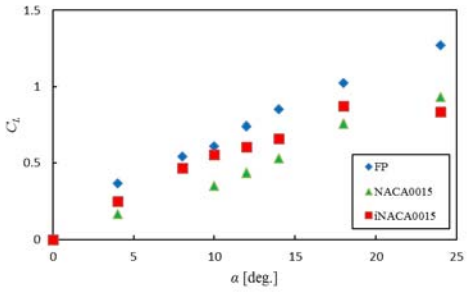

(b) Lift coefficient C_L

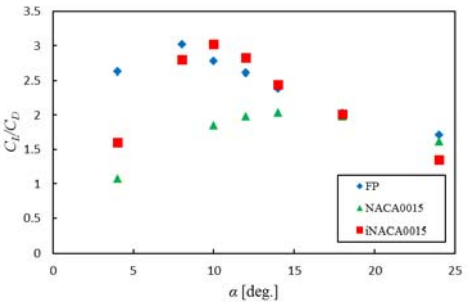

(c) Lift-to-drag ratio C_L/C_D

Fig. 7 Aerodynamic characteristics versus attack angle α at $Re = 8.0\times10^2$. +; 2D Computations by Hirata et al. (2010) (for FP at $Re = 5.0\times10^2$)×and -; 2D Computations by Hirata et al. (for NACA0015 at $Re = 5.0\times10^2$ and $Re = 1.0\times10^3$, respectively). ●; 3D Computations by Hirata et al. (for NACA0015 at $Re = 1.0\times10^3$).

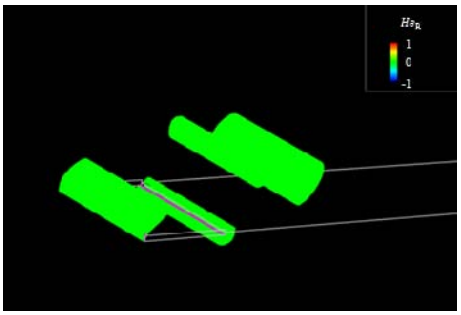

(a) For FP

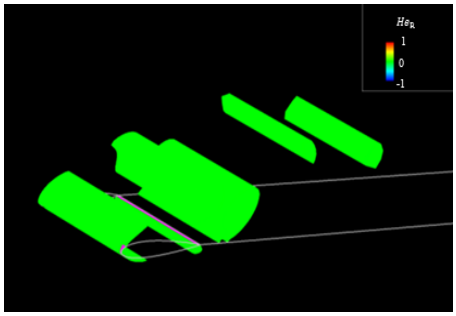

(b) For NACA0015

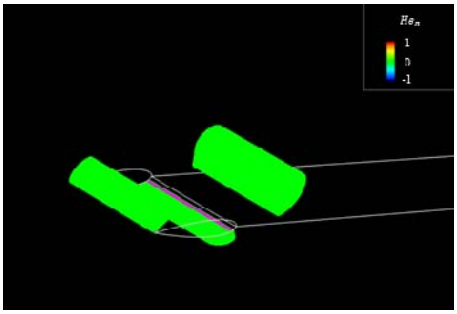

(c) For iNACA0015

Fig. 8 Flow at an instant at $Re = 1.0\times10^2$ and $\alpha = 24$ deg., which is visualized using iso-Q surfaces with a normalized $Q = 3$. The color on the iso-Q surfaces represents the relative helicity He_R, shown as a legend on the upper right hand of each figure.

TSF0015

Now, we consider the influence of α upon the flow around an airfoil. Figures 11 and 12 show the visualized flows at $Re = 8.0\times10^2$. Figure 11 visualizes the flow for the FP using iso-Q surfaces with a normalized Q value ($\equiv Qc^2/U_\infty^2$) of 3. Figure 12 represents the pressure distribution around an airfoil. Pressure p are non-dimensionalized as pressure coefficient C_p.

We indicate the value of C_p by color, with its corresponding color bar on the upper-right hand of each figure. In both Figs. 11 and 12, figures (a), (b), (c) and (d) are at $\alpha = 4$, 10, 18 and 24 deg., respectively. We can see that the flow is steady and two-dimensional at $\alpha = 4$ deg. from Figs. 11(a) and 12(a). At $\alpha = 10$ and 18 deg., the flow is unsteady(periodic) and two-dimensional (in Figs. 11(b) and (c) and 12(b) and (c)). At $\alpha = 24$ deg. the flow is unsteady(periodic with random noise) and three-dimensional(in Figs. 11(d) and 12(d))

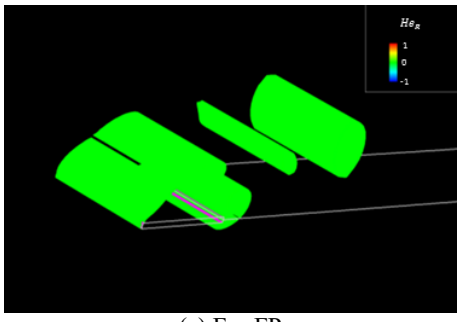

(a) For FP

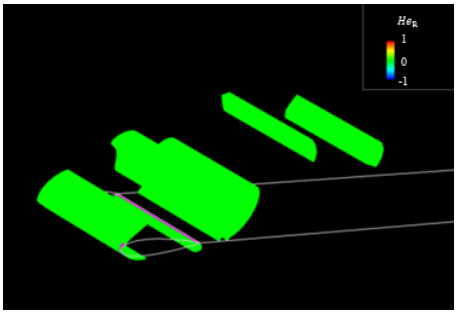

(b) For NACA0015

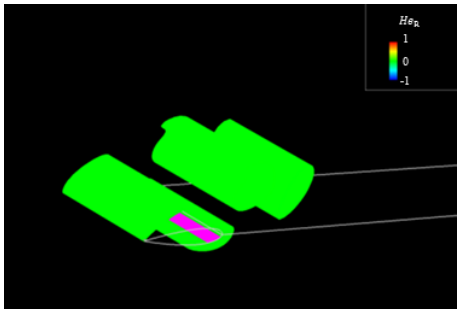

(c) For iNACA0015

Fig. 9 Flow at an instant at $Re = 4.0\times10^2$ and $\alpha = 24$ deg., which is visualized using iso-Q surfaces with a normalized $Q = 3$. The color on the iso-Q surfaces represents the relative helicity He_R shown as a legend on the upper right hand of each figure.

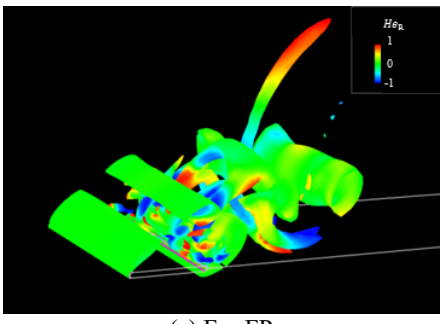

(a) For FP

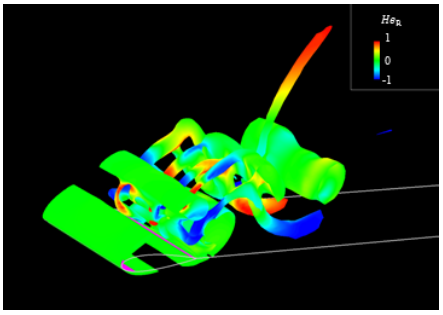

(b) For NACA0015

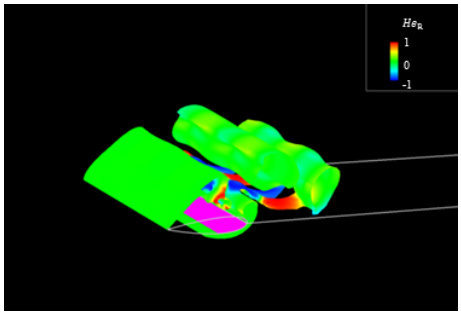

(c) For iNACA0015

Fig. 10 Flow at an instant at $Re = 8.0\times10^2$ and $\alpha = 24$ deg., which is visualized using iso-Q surfaces with a normalized $Q = 3$. The color on the iso-Q surfaces represents the relative helicity He_R shown as a legend on the upper right hand of each figure.

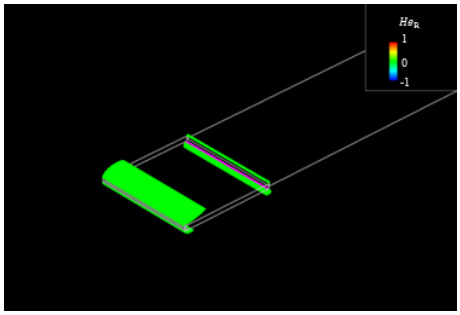

(a) $\alpha = 4$ deg.

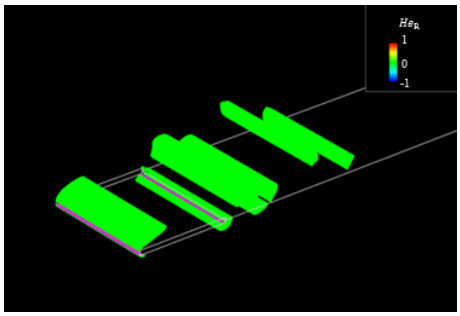

(b) $\alpha = 10$ deg.

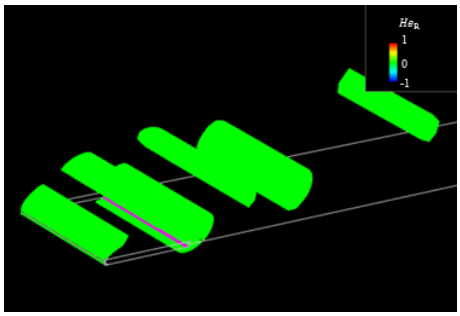

(c) $\alpha = 18$ deg.

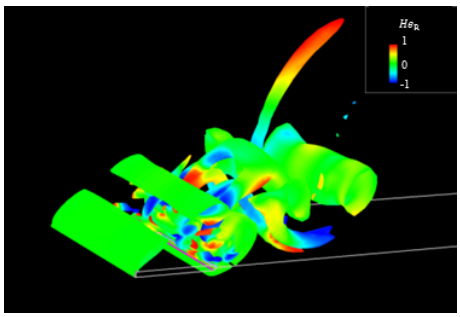

(d) $\alpha = 24$ deg.

Fig. 11 Flow for FP at $Re = 8.0\times10^2$ and $\alpha = 4 - 24$ deg., which is visualized using iso-Q surfaces with normalized $Q = 3$. The color on the iso-Q surfaces represents relative helicity He_R shown as a legend on the upper left hand of each figure.

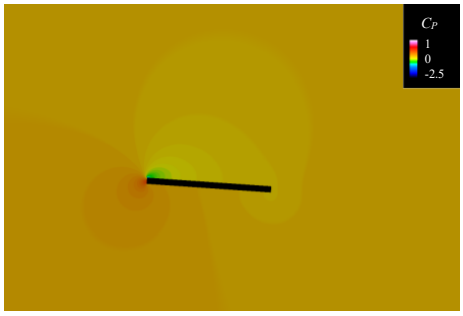

(a) $\alpha = 4$ deg.

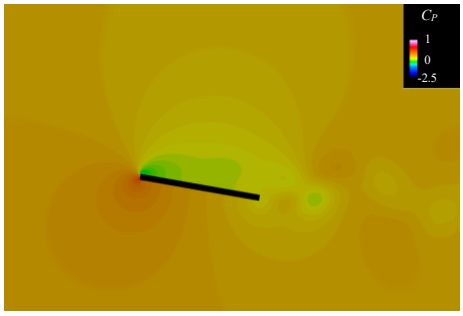

(b) $\alpha = 10$ deg.

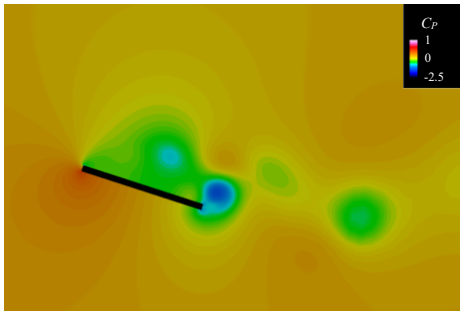

(c) $\alpha = 18$ deg.

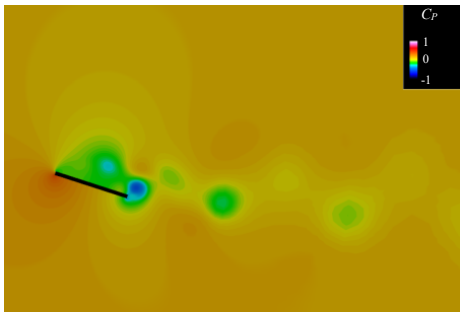

(d) $\alpha = 24$ deg.

Fig. 12 Pressure distribution at an instant for FP at $Re = 8.0\times10^2$ and $\alpha = 4 - 24$ deg. The color represents the pressure coefficient C_p averaged in the spanwise direction.

In addition to we indicate the value of flow line by color, with its corresponding color bar on the upper-right hand of each figure. In Fig. 13 are at $\alpha = 24$ deg.

3.3 Flow visualization by experiment

Finally, in order to confirm the accuracy and reliability of our computers, we compare the computation with our experiment. Figure 14 shows a sample of experiment, the namely velocity vectors by PIV around the airfoil at an instant for FP at $Re = 8.0\times10^2$ and $\alpha = 24$ deg. The figure agrees well with Fig 13.

4. Conclusions

We have investigated three kinds of airfoils, namely, such two basic airfoils as a flat plate and a NACA0015 together with an iNACA0015 (the NACA0015 placed back to front) which was proposed as a high-performance airfoil for low Reynolds number, in a low-Reynolds-number range of $Re = 1.0\times10^2 - 8.0\times10^2$, using three-dimensional computations and experiments. As a result, we have revealed the effects of attack angle α upon various aerodynamic characteristics such as the lift coefficient C_L, drag coefficient C_D and the lift-to-drag ratio C_L/C_D. Besides, we have visualized the flow structure in three dimensions. Concerning the controllability, the NACA0015 is superior among the three airfoils, due to the lack of a remarkable stall feature on C_L/C_D. This suggests the possibility of more-efficient flights with long ranges in actual operations of UAVs/MAVs.

In summary, once we consider both the steadies and two/three-dimensionality, we cannot ignore any of such three factors as Re, α and the geometry of airfoil's section.

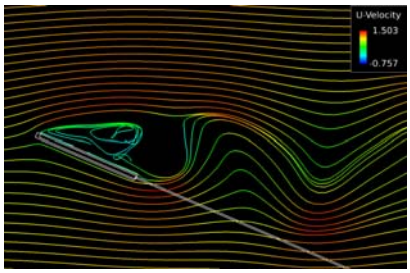

Fig. 13 Flow line at an instant for FP at $Re = 8.0\times10^2$ and $\alpha = 24$ deg.

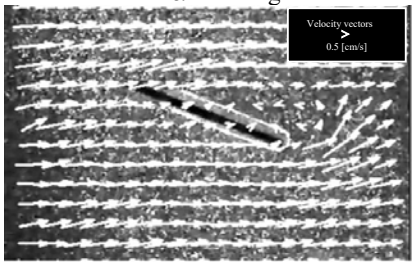

Fig. 14 Velocity vectors at an instant for FP at $Re = 8.0\times10^2$ and $\alpha = 24$ deg.

5. References

[1] Jacobs, E. N. and Sherman, A. (1937). Airfoil Section Characteristics as Affected by Variations in the Reynolds Number, NACA Technical Report, No. 586, pp. 227 – 267.

[2] Abbott, I. H. and Doenhoff, A. E. von. (1958). Theory of Wing Sections, Dover, New York, pp. 462 – 463.

[3] Riegels, F. W. (1961). Aerofoil Sections, Butterworths, London.

[4] Eppler, R. (1990). Airfoil Design and Data, Springer-Verlag, Berlin.

[5] Kawano, H. (2007). Three-Dimensional Obstacle Avoidance of Blimp-Type Unmanned Aerial Vehicle Flying in Unknown and Non-Uniform Wind Disturbance, *Journal of Robotics and Mechatronics*, Vol. 19, No. 2, 2007, pp. 166 – 173.

[6] Iwata, K., Matsubara, K., Kawasaki, K. and Matsumoto, O. (2012). Turbojet Engine for Aerial Cargo Robot (ACR), *Journal of Robotics and Mechatronics*, Vol. 24, No. 6, 2012, pp. 1040 – 1045.

[7] McMasters, J. H. and Henderson, M. L. (1980). Low Speed Single Element Airfoil Synthesis, Tech. Soaring, Vol. 6, 1980, pp. 1 – 21.

[8] Okamoto, M. Yasuda, K. and Azuma, A. (1996). Aerodynamic Characteristics of the Wings and Body of a Dragonfly, *Journal of Experimental Biology*, Vol. 199, 1996, pp. 281 – 294.

[9] Abe, H., Tutui, Y. and Yoshiki, H. (1996). Aerodynamic Characteristics of an Airfoil in Turbulent and Low-Reynolds-Number Flows: Experiments with a Jet Grid, *Transactions of the Japan Society of Mechanical Engineers Series B*, Vol. 62 , No. 602, 1996, pp. 3592 – 3598, (in Japanese).

[10] Sunada, S., Sakaguchi, A. and Kawachi, K. (1997). Airfoil Section Characteristics at a Low Reynolds Number, Transactions ASME, *Journal of Fluids Engineering*, Vol. 199, 1997, pp. 129 – 135.

[11] Abe, H. (2000). Aerodynamic Characteristics of an Airfoil in Turbulent and Low-Reynolds-Number Flows, *Technical Report of Mechanical Engineering Laboratory*, AIST, Vol. 186, 2000 (in Japanese).

[12] Isikawa, H., Kudo, D., Kiya, M., Mochizuki, O. and Zheng, Z. (2001). Aerodynamic Characteristics of a Flat-Plate Wing with Leading-Edge Serrations, *Transactions of the Japan Society of Mechanical Engineers, Series B*, Vol. 67, No. 655, 2001, pp. 680 – 687, (in Japanese).

[13] Motohashi, T. (2001). Characteristics of Rectangular Wings at Low Reynolds Numbers,

Proc. 39th Aircraft Symposium, JSASS, Paper No. 3D6, 2001, pp. 1 – 4, (in Japanese).

[14] Nakane, N., Tanaka.T. and Motohashi, T. (2003). Aerodynamic Characteristics of NACA0012 in a Wide Reynolds Number range, *Proc. 35th Fluid Dynamics Conference*, JSASS, 2003, pp. 179 – 182, (in Japanese).

[15] Sun, Q. and Boyd, I. D. (2004). Flat-Plate Aerodynamics at Very Low Reynolds Number, *Journal of Fluid Mechanics*, Vol. 502, 2004, pp. 199 – 206.

[16] Takagi, R. (2006). Aerodynamic Characteristics of NACA4402 in Low Reynolds Number Flows, *Journal of the Japan Society for Aeronautical and Space Sciences*, Vol. 54, No. 631, 2006, pp. 367 – 373, (in Japanese).

[17] Ohtake, T., Nakae, Y. and Motohashi, T. (2007). Nonlinearity of the Aerodynamic Characteristics of NACA0012 Aerofoil at Low Reynolds Numbers, *Journal of the Japan Society for Aeronautical and Space Sciences*, Vol. 55, No. 644, 2007, pp. 439 – 445, (in Japanene).

[18] Yagi, H. and Kawahara, M. (2007). Optimal Shape Determination of a Body Located in Incompressible Viscous Fluid Flow, *Computer Methods in Applied Mechanical and Engineering*, Vol. 196, 2007, pp. 5084 – 5091.

[19] Katamine, E., Nishihashi, N. and Azegami, H. (2008). Shape Optimization of Steady-State Viscous Flow Fields for Drag Minimization and Lift Maximization, *Transactions of the Japan Society of Mechanical Engineers, Series B*, Vol. 74, No. 748, 2008, pp. 2426 – 2433, (in Japanese).

[20] Ohtake, T. and Motohashi, T. (2009). Flow Field around NACA0012 Airfoil at Low Reynolds Numbers, *Journal of the Japan Society for Aeronautical and Space Sciences*, Vol. 57, 2009, pp. 397 – 404, (in Japanene).

[21] Taira, K. and Colonius, T. (2009). Three-Dimensional Flows Around Low-Aspect-Ratio Flat-Plate Wings at Low Reynolds Numbers, *Journal of Fluid Mechanics*, Vol. 623, 2009, pp. 187 – 207.

[22] Hirata, K., Kawakita, M., Iijima, T., Koga, M., Kihira, M. and Funaki, J. (2010). Numerical and Experimental Study on Aerodynamic Characteristics of Basic Airfoils at Low Reynolds Numbers, *Journal of Fluid Science and Technology*, Vol. 5, 2010, pp. 447 – 463.

[23] Zhou, Y., Md. Mahbub Alam, Yang, H. X., Guo, H. and Wood, D. H. (2011). Fluid Forces on a Very Low Reynolds Number Airfoil and Their Prediction, *International Journal of Heat and Fluid Flow*, Vol. 32, 2011, pp. 329 – 339.

[24] Ebata, S., Yasuda, T., Minagawa, H., Miyamoto, Y. and Satofuka, N. (2013). A Study of Cross-Sectional Shape of Wing for Underwater Glider at Low Reynolds Number Region, *Transactions of the Japan Society of Mechanical Engineers Series B*, Vol. 79, No. 806, 2013, pp. 12 – 25, (in Japanene).

[25] Hirata, K., Nozawa, R., Kondo, S., Onishi, K. and Tanigawa, H. (2016). On High-Performance Airfoil at Very Low Reynolds Number, *Journal of Robotics and Mechatronics*, Vol. 28, No. 3, 2016, pp. 273 – 285.